Thermal broadening of the J-band in disordered linear molecular aggregates

Heijs, D.J.; Malyshev, V.A.; Knoester, Jasper

Published in:
Journal of Chemical Physics

DOI:
10.1063/1.2052591

Publication date:
2005

Thermal broadening of the *J*-band in disordered linear molecular aggregates: A theoretical study

D. J. Heijs, V. A. Malyshev,[a] and J. Knoester[b]
Institute for Theoretical Physics and Materials Science Center, University of Groningen, Nijenborgh 4, 9747 AG Groningen, The Netherlands

(Received 22 June 2005; accepted 10 August 2005; published online 11 October 2005)

We theoretically study the temperature dependence of the *J*-band width in disordered linear molecular aggregates, caused by dephasing of the exciton states due to scattering on vibrations of the host matrix. In particular, we consider inelastic one- and two-phonon scatterings between different exciton states (energy-relaxation-induced dephasing), as well as the elastic two-phonon scattering of the excitons (pure dephasing). The exciton states follow from numerical diagonalization of a Frenkel exciton Hamiltonian with diagonal disorder; the scattering rates between them are obtained using the Fermi golden rule. A Debye-type model for the one- and two-phonon spectral densities is used in the calculations. We find that, owing to the disorder, the dephasing rates of the individual exciton states are distributed over a wide range of values. We also demonstrate that the dominant channel of two-phonon scattering is not the elastic one, as is often tacitly assumed, but rather comes from a similar two-phonon inelastic scattering process. In order to study the temperature dependence of the *J*-band width, we simulate the absorption spectrum, accounting for the dephasing-induced broadening of the exciton states. We find a power-law (T^p) temperature scaling of the effective homogeneous width, with an exponent p that depends on the shape of the spectral density of the host vibrations. In particular, for a Debye model of vibrations, we find $p \approx 4$, which is in good agreement with the experimental data on *J* aggregates of pseudoisocyanine [I. Renge and U. P. Wild, J. Phys. Chem. A, **101**, 7977 (1997)]. © *2005 American Institute of Physics*. [DOI: 10.1063/1.2052591]

I. INTRODUCTION

Ever since the discovery of aggregation of cyanine dye molecules by Jelley[1] and Scheibe[2] the width of the absorption band of these linear aggregates (the *J*-band) has attracted much attention. At low temperatures, the *J*-band may be as narrow as a few tens of cm^{-1} (for pseudoisocyanine), while at room temperature it is typically a few hundred cm^{-1}.[3] The small width at low temperature is generally understood as resulting from the excitonic nature of the optical excitations,[4] which leads to exchange narrowing of the inhomogeneous broadening of the transitions of individual molecules.[5] As the optically dominant exciton states in inhomogeneous *J* aggregates occur below the exciton band edge, their vibration-induced dephasing is strongly suppressed at low temperatures. Thus, the *J*-band is inhomogeneously broadened, except for a small residual homogeneous component (~ 0.1 cm^{-1}) caused by spontaneous emission of the individual exciton states underlying the spectrum. Upon increasing the temperature, the vibration-induced dephasing of the exciton states increases, the *J*-band broadens, and obtains a more homogeneous character.

Over the past 20 years, the temperature dependence of the *J*-band width and the homogeneous broadening of the exciton states, has been studied by several authors. In 1987, de Boer *et al.*[6] performed accumulated-echo experiments to study the temperature dependence of the pure dephasing time in *J* aggregates of pseudoisocyanine bromide (PIC-Br) and found that within the temperature range of 1.5–100 K, this time is linearly proportional to the occupation number of a mode with an energy of 9 cm^{-1}. They assigned this to a librational mode of the aggregate. Later on, Fidder *et al.*[7] (see also Refs. 8 and 9) showed that a similar study carried out over a wider temperature range, 1.5–190 K, required the occupation numbers of three vibration modes at 9, 305, and 973 cm^{-1}. Using the hole burning technique, Hirschmann and Friedrich[10] studied the homogeneous width of the exciton states in pseudoisocyanine iodide (PIC-I) over the temperature range of 350 mK–80 K. They were able to fit their measurements by a superposition of two exponentials, with activation energies of 27 and 330 cm^{-1}, and they attributed the broadening to scattering of the excitons on an acoustic mode and optical mode, respectively, of the aggregate. Finally, in 1997 Renge and Wild[11] measured the temperature dependent width $\Delta(T)$ of the total *J*-band of pseudoisocyanine chloride (PIC-Cl) and fluoride (PIC-F) over the wide temperature range of 10–300 K. They found that over this entire range their data closely obeyed a power-law dependence $\Delta(T)=\Delta(0)+bT^p$ with the exponent $p=3.4$. They suggested the scattering of the excitons on host vibrations as a possible source of this behavior.

The above overview clearly demonstrates that the temperature dependence of the most important characteristic of *J*

[a]On leave from S.I. Vavilov State Optical Institute, Birzhevaya Liniya 12, 199034 Saint-Petersburg, Russia.
[b]Electronic mail: j.knoester@rug.nl

aggregates, namely, the *J*-band, is not understood. It is even not clear what is the source of thermal broadening: dephasing due to vibrational modes of the aggregate itself or due to modes of the host matrix. Theoretically, the study of the exciton dephasing in *J* aggregates is complicated by the fact that static disorder plays an important role in these systems, as is clear from the strongly asymmetric low-temperature line shape.[8,9] The simultaneous treatment of disorder, leading to exciton localization and scattering on vibrational modes, is a problem that requires extensive numerical simulations. Such simulations have been used previously to model the optical response of polysilanes,[12,13] the temperature-dependent fluorescence[14] and transport[15] properties of *J* aggregates, and single molecular spectroscopy of circular aggregates.[16] Alternatively, stochastic models have been applied to describe the scattering of excitons on vibrations in disordered aggregates and the resulting spectral line shape[17,18] and relaxation dynamics.[19]

In this paper, we report on a systematic theoretical study of dephasing of weakly localized Frenkel excitons in one-dimensional systems, focusing on the effect of the scattering of the excitons on the vibrational modes (phonons) of the host. For a chainlike configuration it seems physically reasonable to assume that the coupling to host vibrations dominates the dynamics of the excitons. For coupling to vibrations in the chain, one expects self-trapped exciton states,[20] for which in most aggregates no clear signature is found. We describe the phonons by a Debye model and consider one-phonon as well as (elastic and inelastic) two-phonon contributions to the dephasing. The scattering rates between the various, numerically obtained, exciton states are derived using the Fermi golden rule. Due to the disorder, the dephasing rates of individual exciton states are distributed over a wide range, in particular, at low temperature, making it meaningless to associate the width of individual exciton levels with the *J*-band width. Rather, this width is determined by direct simulation of the total absorption spectrum and is found to scale with temperature according to a power law.

The outline of this paper is as follows: In Sec. II we introduce the Hamiltonian for excitons in a disordered chain and coupled to host vibrations. General expressions for the exciton dephasing rates are derived in Sec. III. Section IV deals with the temperature dependence of the dephasing rates for the disorder-free case, where analytical expressions can be obtained. In Sec. V we give the results of our numerical simulations for the dephasing rates in the presence of disorder and analyze their temperature dependence and fluctuations as well as the total *J*-band width. We compare to experiment in Sec. VI and discuss an alternative mechanism of dephasing due to the coupling of excitons to a local vibration. In Sec. VII we present our conclusions.

II. MODEL

We consider an ensemble of *J* aggregates embedded in a disordered host matrix. The aggregates are assumed to be decoupled from each other, while they interact with the host. A single aggregate is modeled as an open linear chain of *N* coupled two-level monomers with parallel transition dipoles. The interaction between a particular monomer and the surrounding host molecules in the equilibrium configuration leads to shifts in the monomer's transition energy. Due to the host's structural disorder, this shift is different for each monomer in the aggregate, giving rise to on-site (diagonal) disorder. Moreover, the vibrations of the host couple to the aggregate excited states, because the associated displacements away from the equilibrium configuration dynamically affect the monomer transition energies. Accounting for these shifts up to second order in the molecular displacements, the resulting Hamiltonian in the site representation reads,

$$H = H^{\mathrm{ex}} + H^{\mathrm{bath}} + V^{(1)} + V^{(2)}, \tag{1a}$$

with

$$H^{\mathrm{ex}} = \sum_{n=1}^{N} \varepsilon_n |n\rangle\langle n| + \sum_{n,m=1}^{N} J_{nm} |n\rangle\langle m|, \tag{1b}$$

$$H^{\mathrm{bath}} = \sum_{q} \omega_q a_q^{\dagger} a_q, \tag{1c}$$

$$V^{(1)} = \sum_{n=1}^{N} \sum_{q} V_{nq}^{(1)} |n\rangle\langle n| (a_q + a_q^{\dagger}), \tag{1d}$$

$$V^{(2)} = \sum_{n=1}^{N} \sum_{qq'} V_{nqq'}^{(2)} |n\rangle\langle n| (a_q + a_q^{\dagger})(a_{q'} + a_{q'}^{\dagger}). \tag{1e}$$

Here, H^{ex} is the bare Frenkel exciton Hamiltonian, with $|n\rangle$ denoting the state in which the nth monomer is excited and all the other monomers are in the ground state. The monomer excitation energies, $\varepsilon_1, \varepsilon_2, \ldots, \varepsilon_N$, are uncorrelated stochastic Gaussian variables, with mean $\bar{\varepsilon}$ and standard deviation σ, referred to as the disorder strength. Hereafter, $\bar{\varepsilon}$ is set to zero. The resonant interactions J_{nm} are considered to be nonrandom and are assumed to be of dipolar origin: $J_{nm} = -J/|n-m|^3$ ($J_{nn} \equiv 0$), with $J > 0$ denoting the nearest-neighbor coupling.

H^{bath} describes the vibrational modes of the host, labeled q and with the spectrum ω_q ($\hbar = 1$). The operator a_q ($a_q^{\dagger}$) annihilates (creates) a vibrational quantum in mode q. Finally, the operators $V^{(1)}$ and $V^{(2)}$ describe the linear and quadratic exciton-vibration couplings, respectively, where the quantities $V_{nq}^{(1)}$ and $V_{nqq'}^{(2)}$ indicate their strengths. We do not derive explicit expressions for these coupling strengths, as we aim to treat them on a phenomenological basis. In particular, owing to the disordered nature of the host, we consider these strengths stochastic quantities, for which we only specify the following stochastic properties with respect to the site index n,

$$\langle V_{nq}^{(1)} \rangle = \langle V_{nqq'}^{(2)}, \rangle = 0, \tag{2a}$$

$$\langle V_{mq}^{(1)} V_{nq}^{(1)*} \rangle = \delta_{mn} |V_q^{(1)}|^2, \tag{2b}$$

$$\langle V_{mqq'}^{(2)}, V_{nqq'}^{(2)*} \rangle = \delta_{mn} |V_{qq'}^{(2)},|^2, \tag{2c}$$

where the angular brackets denote averaging over realizations of $V_{nq}^{(1)}$ and $V_{nqq'}^{(2)}$. The Kronecker symbol in Eqs. (2b) and (2c) implies that the surroundings of different monomers in the aggregate are not correlated.

In general, the Hamiltonian [Eq. (1)] cannot be diagonalized analytically. If the exciton-vibration coupling is not too strong, the method of choice is first to find the exciton eigenstates by numerical diagonalization and then to consider the scattering on the basis of these eigenstates. Explicitly, the exciton states follow from the eigenvalue problem,

$$\sum_{m=1}^{N} H_{nm}^{\mathrm{ex}} \varphi_{\nu m} = E_\nu \varphi_{\nu n}, \quad \nu = 1,2,\ldots,N, \tag{3a}$$

where $H_{nm}^{\mathrm{ex}} = \langle n|H^{\mathrm{ex}}|m\rangle$ and E_ν is the eigenenergy of the exciton state $|\nu\rangle$,

$$|\nu\rangle = \sum_{n=1}^{N} \varphi_{\nu n}|n\rangle. \tag{3b}$$

In the exciton representation, the exciton-vibration interactions take the form

$$V^{(1)} = \sum_{\mu,\nu=1}^{N} \sum_{q} V_{\mu\nu q}^{(1)} |\mu\rangle\langle\nu|(a_q + a_q^\dagger), \tag{4a}$$

$$V^{(2)} = \sum_{\mu,\nu=1}^{N} \sum_{qq'} V_{\mu\nu qq'}^{(2)} |\mu\rangle\langle\nu|(a_q + a_q^\dagger)(a_{q'} + a_{q'}^\dagger), \tag{4b}$$

where $V_{\mu\nu q}^{(1)}$ and $V_{\mu\nu qq'}^{(2)}$ are the matrix elements of the vibration-induced scattering of an exciton from state $|\nu\rangle$ to state $|\mu\rangle$, given by

$$V_{\mu\nu q}^{(1)} = \sum_{n=1}^{N} V_{nq}^{(1)} \varphi_{\mu n} \varphi_{\nu n}, \tag{5a}$$

$$V_{\mu\nu qq'}^{(2)} = \sum_{n=1}^{N} V_{nqq'}^{(2)} \varphi_{\mu n} \varphi_{\nu n}. \tag{5b}$$

Spectroscopic data on *J* aggregates clearly reveal that the exciton-vibration coupling in these systems is usually weak. For the prototypical *J* aggregates of PIC, this claim is corroborated by two facts: (i) the narrowness of the *J*-band, which only is a few tens of cm^{-1} at liquid-helium temperature and becomes several times broader at room temperature, and (ii) the absence of a fluorescence Stokes shift of the *J*-band (see, e.g., Ref. 7). The extended nature of the exciton states in *J* aggregates helps to reduce the exciton-vibration coupling, as it leads to averaging of the static as well as the dynamic fluctuations of the site energies, effects known as exchange[5] and motional[21,22] narrowing, respectively. The weakness of the exciton-vibration coupling allows one to calculate the scattering and dephasing rates of the excitons through perturbation theory. This analysis is presented in Sec. III.

III. DEPHASING RATES

Following the arguments given at the end of Sec. II, we will use Fermi's golden rule to calculate the rate for scattering of excitons from one localized state $|\nu\rangle$ to another one $|\mu\rangle$. The result reads

$$W_{\mu\nu}^{(\xi)} = 2\pi \sum_{f} \sum_{i} \rho(\Omega_i) \langle |\langle \mu, f|V^{(\xi)}|\nu, i\rangle|^2 \rangle \times \delta(E_\mu - E_\nu + \Omega_f - \Omega_i). \tag{6}$$

Here, the superscript $\xi = 1,2$ distinguishes between one- and two-vibration-assisted exciton scatterings. Furthermore, Ω_i and Ω_f are the energies of the vibration bath in the initial ($|i\rangle = |\{n_q\}_i\rangle$) and final ($|f\rangle = |\{n_q\}_f\rangle$) states, respectively, where $\{n_q\}$ denotes the set of occupation numbers of the vibrational modes. The quantity $\rho(\Omega_i)$ is the equilibrium density matrix of the initial state of the bath. Finally, the angular brackets indicate that we average over the stochastic realizations of the surroundings of each monomer in the aggregate.

A. Linear exciton-vibration coupling

In a one phonon-assisted scattering process, the occupation number of one phonon mode q increases or decreases by one, corresponding to the emission and absorption of a vibrational quantum, respectively. Consequently, $\Omega_f - \Omega_i = \pm\omega_q$. Substituting the explicit form of the operator $V^{(1)}$ from Eq. (1d) into Eq. (6), we obtain

$$W_{\mu\nu}^{(1)} = 2\pi \sum_{n=1}^{N} \varphi_{\mu n}^2 \varphi_{\nu n}^2 \sum_{q} |V_q^{(1)}|^2 [[\bar{n}(\omega_q) + 1]\delta(\omega_{\mu\nu} + \omega_q) + \bar{n}(\omega_q)\delta(\omega_{\mu\nu} - \omega_q)], \tag{7}$$

where $\bar{n}(\omega_q) = [\exp(\omega_q/T) - 1]^{-1}$ is the mean occupation number of the vibrational mode q (the Boltzmann constant $k_B = 1$) and $\omega_{\mu\nu} = E_\mu - E_\nu$. In deriving Eq. (7), we used the properties of the stochastic function $V_{nq}^{(1)}$ given by Eqs. (2a) and (2b). Defining the one-vibration spectral density as

$$\mathcal{F}^{(1)}(\omega) \equiv 2\pi \sum_{q} |V_q^{(1)}|^2 \delta(\omega - \omega_q), \tag{8}$$

we can rewrite Eq. (7) in the form

$$W_{\mu\nu}^{(1)} = \sum_{n=1}^{N} \varphi_{\mu n}^2 \varphi_{\nu n}^2 \mathcal{F}^{(1)}(|\omega_{\mu\nu}|) \times \begin{cases} \bar{n}(\omega_{\mu\nu}), & \omega_{\mu\nu} > 0, \\ \bar{n}(-\omega_{\mu\nu}) + 1, & \omega_{\mu\nu} < 0. \end{cases} \tag{9}$$

As we observe, the rate $W_{\mu\nu}^{(1)}$ is proportional to the overlap integral of the site occupation probabilities, $\varphi_{\mu n}^2$ and $\varphi_{\nu n}^2$, of the exciton states involved. First of all, this leads to a strong suppression of the scattering rate if states $|\mu\rangle$ and $|\nu\rangle$ overlap weakly or not at all. Second, as the low-energy exciton states in a disordered chain exhibit large fluctuations in their localization size,[23] also the scattering rates may undergo large fluctuations (see Sec. V).

The dependence of $W_{\mu\nu}^{(1)}$ on the energy mismatch $\omega_{\mu\nu}$ is determined by the one-phonon spectral density $\mathcal{F}^{(1)}(\omega)$. Characterizing this function requires knowledge of the vibra-

tional spectrum ω_q as well as the q dependence of the exciton-vibration coupling $V_q^{(1)}$. For the special case of scattering on acoustic phonons of a relatively long wavelength, we have $\mathcal{F}^{(1)}(\omega) \sim \omega^3$. This behavior results from the ω^2 dependence of the density of states of acoustic phonons, combined with the fact that in the long-wavelength limit $|V_q^{(1)}|^2 \sim \omega_q$.[24,25] One may consider this a Debye-type model, in which one replaces the summation over the mode index q by an integration over the frequency ω_q according to the well-known rule,

$$\sum_q \rightarrow C \int_0^{\omega_c} d\omega_q \omega_q^2. \tag{10}$$

Here, C is an irrelevant constant, which we will incorporate in an overall free parameter (see below), and ω_c is a cutoff frequency. It is important to note that ω_c is not necessarily related to the Debye frequency: the generally very complex density of vibrational states in a disordered solid may on average exhibit an ω^2 scaling up to a given frequency ω_c.

Inspired by the above, we consider a slightly wider class of one-phonon spectral densities, given by

$$\mathcal{F}^{(1)}(\omega) = W_0^{(1)} \left(\frac{\omega}{J} \right)^{\alpha} \Theta(\omega_c - \omega). \tag{11}$$

Here, $W_0^{(1)}$ is a free parameter in the model, which characterizes the overall strength of the one-vibration-assisted scattering rates. It absorbs a number of other parameters characteristic for the host lattice (such as the velocity of sound), the constant C from Eq. (10), as well as the strength of the transfer interaction J (for details, see Ref. 25). $\Theta(x)$ is the Heaviside step function. When performing numerical simulations, we will mostly use $\alpha=3$, for which the spectral density of acoustic phonons in the long-wave limit is recovered. In some instances, however, we will discuss how the results depend on the exponent α.

Several observations support considering a Debye-type vibration spectral density, even for a disordered host. Thus, for strongly disordered Yb^{3+}-doped phosphate glasses, a parabolic behavior of the one-phonon spectral density was found over a rather wide range of measurement ($0-100\ \mathrm{cm}^{-1}$).[26] Furthermore, the closely related spectral densities of the form $\mathcal{F}^{(1)}(\omega) \sim (\omega/\omega_c)^{\alpha} \exp(-\omega/\omega_c)$ (or linear combinations of such functions) have been used successfully to fit the optical dynamics in photosynthetic antenna complexes (see, e.g., Refs. 27–30).

One-phonon-assisted scattering results in the transition of an exciton from a given state $|\nu\rangle$ to state $|\mu\rangle$, where necessarily $\mu \neq \nu$. In other words, this type of scattering changes the occupation probabilities of the exciton states and thus causes population (or energy) relaxation. The population relaxation in turn contributes to the dephasing of state $|\nu\rangle$. The corresponding dephasing rate is given by (see, e.g., Ref. 31)

$$\Gamma_{\nu}^{(1)} \equiv \frac{1}{2} \sum_{\mu(\neq\nu)} W_{\mu\nu}^{(1)}. \tag{12}$$

Thus, $\Gamma_{\nu}^{(1)}$ represents the one-phonon-assisted contribution to the homogeneous broadening of the excitonic level ν. We note that the $\Gamma_{\nu}^{(1)}$ indirectly depend on temperature through the $\bar{n}(\omega_{\mu\nu})$ [cf. Eq. (9)]. The temperature dependence of the sum over the scattering rates in Eq. (12) and the corresponding width of the total exciton absorption spectrum will be analyzed in Secs. IV and V.

B. Quadratic exciton-phonon coupling

When excitons scatter on the second-order displacements of the host molecules, described by the operator $V^{(2)}$, the occupation numbers of two phonon modes q and q' with frequencies ω_q and $\omega_{q'}$ change by ± 1. Thus, $\Omega_f - \Omega_i = \pm\omega_q \pm \omega_{q'}$, where any combination of plus and minus is allowed. The corresponding scattering rates $W_{\mu\nu}^{(2)}$ are obtained from Eq. (6), taking into account the stochastic properties of $V_{nqq'}^{(2)}$, given by Eqs. (2a) and (2c),

$$\begin{aligned} W_{\mu\nu}^{(2)} = 2\pi \sum_{n=1}^{N} \varphi_{\mu n}^2 \varphi_{\nu n}^2 \sum_{qq'} |V_{qq'}^{(2)}|^2 \\ \times [[\bar{n}(\omega_q)+1][\bar{n}(\omega_{q'})+1]\delta(\omega_{\mu\nu}+\omega_q+\omega_{q'}) \\ + 2\bar{n}(\omega_q)[\bar{n}(\omega_{q'})+1]\delta(\omega_{\mu\nu}-\omega_q+\omega_{q'}) \\ + \bar{n}(\omega_q)\bar{n}(\omega_{q'})\delta(\omega_{\mu\nu}-\omega_q-\omega_{q'})]. \end{aligned} \tag{13}$$

If in analogy to the one-vibration-assisted scattering, we define the two-vibration spectral density $\mathcal{F}^{(2)}(\omega,\omega')$ as

$$\mathcal{F}^{(2)}(\omega,\omega') \equiv 2\pi \sum_{qq'} |V_{qq'}^{(2)}|^2 \delta(\omega-\omega_q)\delta(\omega'-\omega_{q'}), \tag{14}$$

the scattering rate $W_{\mu\nu}^{(2)}$ takes the form

$$\begin{aligned} W_{\mu\nu}^{(2)} = \sum_{n=1}^{N} \varphi_{\mu n}^2 \varphi_{\nu n}^2 \int d\omega d\omega' \mathcal{F}^{(2)}(\omega,\omega')[[\bar{n}(\omega)+1] \\ \times [\bar{n}(\omega')+1]\delta(\omega_{\mu\nu}+\omega+\omega') + 2\bar{n}(\omega)[\bar{n}(\omega')+1] \\ \times \delta(\omega_{\mu\nu}-\omega+\omega') + \bar{n}(\omega)\bar{n}(\omega')\delta(\omega_{\mu\nu}-\omega-\omega')]. \end{aligned} \tag{15}$$

Similar to $\mathcal{F}^{(1)}(\omega)$ [Eq. (8)], we will use a parametrization,

$$\mathcal{F}^{(2)}(\omega,\omega') = \frac{W_0^{(2)}}{J} \left(\frac{\omega\omega'}{J^2} \right)^{\alpha} \Theta(\omega_c-\omega)\Theta(\omega_c-\omega'), \tag{16}$$

where $W_0^{(2)}$ is a free parameter that characterizes the overall strength of the two-vibration-assisted scattering rates [cf. $W_0^{(1)}$ and the discussion following Eq. (11)].

Two main types of two-phonon-assisted processes may be distinguished. Similarly to the one-phonon case, an inelastic channel exists, where scattering occurs between different exciton states, thus giving rise to population relaxation. However, also an elastic channel is present, in which an exciton is scattered by emitting and absorbing a phonon of the same energy, and the final exciton state is identical to the initial one. This process results in pure dephasing of the exciton state, with a rate given by

$$W_{\nu\nu}^{(2)} = 2\sum_{n=1}^{N} \varphi_{\nu n}^4 \int d\omega \mathcal{F}^{(2)}(\omega,\omega)\bar{n}(\omega)[\bar{n}(\omega)+1]. \tag{17}$$

The quantity $\Sigma_{n=1}^{N}\varphi_{\nu n}^4$ is recognized as the inverse participation ratio,[32] which is inversely proportional to the localization size of the exciton state $|\nu\rangle$. Thus, we see that the pure dephasing is suppressed for more extended states, an effect known as the motional narrowing.[21,22]

Like in the one-phonon assisted process, the scattering rate between different states $|\nu\rangle$ and $|\mu\rangle$ is proportional to the overlap of their site occupations. The final expressions for the rates $W_{\mu\nu}^{(2)}$ resulting from Eqs. (15) and (16) are derived in the Appendix; they depend on the sign of $\omega_{\mu\nu}$ as well as on the relation between $|\omega_{\mu\nu}|$ and ω_c. Distinction is made between three inelastic channels: downward ($\downarrow\downarrow$), in which two phonons are emitted, cross ($\uparrow\downarrow$), in which one phonon is absorbed and another is emitted, and upward ($\uparrow\uparrow$), in which two phonons are absorbed. The fourth type of scattering is the elastic (pure dephasing) channel, discussed above already. When calculating the two-phonon-assisted dephasing rate $\Gamma_{\nu}^{(2)}$ of state $|\nu\rangle$, we will account for elastic as well as inelastic contributions,

$$\Gamma_{\nu}^{(2)} = \frac{1}{2}\left[W_{\nu\nu}^{(2)} + \sum_{\mu(\neq\nu)} W_{\mu\nu}^{(2)} \right]. \tag{18}$$

This rate depends on temperature as a result of the mean occupation numbers $\bar{n}(\omega)$ and $\bar{n}(\omega')$ of the vibrational modes.

IV. DISORDER-FREE AGGREGATE

In order to gain insight in the temperature dependence of the dephasing rates and the absorption bandwidth, it is useful to start by considering a homogeneous aggregate, i.e., $\sigma=0$. Analytical results can then be obtained if we restrict the resonant interactions J_{nm} to nearest-neighbor ones. In this approximation (which we will relax in our numerical analysis), we have

$$\varphi_{\nu n} = \left(\frac{2}{N+1}\right)^{1/2} \sin\frac{\pi\nu n}{N+1}, \tag{19a}$$

$$E_{\nu} = -2J\cos\frac{\pi\nu}{N+1}. \tag{19b}$$

The corresponding overlap integrals occurring in Eqs. (7) and (13) now read

$$\sum_{n=1}^{N} \varphi_{\mu n}^2 \varphi_{\nu n}^2 = \frac{1}{N+1}\left[1 + \frac{1}{2}(\delta_{\mu\nu} + \delta_{\mu+\nu,N+1}) \right]. \tag{20}$$

A. One-phonon-assisted dephasing

In a homogeneous linear chain, the lowest exciton state, $|\nu=1\rangle$, contains almost all oscillator strength, thus dominating the absorption spectrum.[5,7] Therefore, the dephasing rate of this state, $\Gamma_1^{(1)}$, is of primary interest. As follows from Eq. (12), it is determined by the sum over the scattering rates to the other exciton states ($\mu\neq 1$), all of which are higher in energy.

In order to evaluate $\Gamma_1^{(1)}$, we replace the summation in Eq. (12) by an integration, $(\Sigma_{\mu} \rightarrow [(N+1)/\pi]\int dK)$, which is allowed if $N\gg 1$ and $T\gg E_2-E_1$. We will also assume that $T\ll J$, which implies that the relevant exciton levels are those near the lower exciton band edge, where $E_{\mu}=-2J+JK^2$ with $K=\pi\mu/(N+1)$. Changing the integration variable to $x=JK^2/T$, using $E_{\mu}-E_1\approx JK^2$ and replacing the lower integration limit $\pi/(N+1)$ by zero, we obtain

$$\Gamma_1^{(1)} = \frac{W_0^{(1)}}{4\pi}\left(\frac{T}{J}\right)^{\alpha+1/2} \int_0^{\omega_c/T} dx \frac{x^{\alpha-1/2}}{e^x-1}. \tag{21}$$

For temperatures $T\ll\omega_c$, the upper integration limit may be extended to infinity, and we arrive at

$$\Gamma_1^{(1)} = \frac{W_0^{(1)}}{4\pi}\Gamma\left(\alpha+\frac{1}{2}\right)\zeta\left(\alpha+\frac{1}{2}\right)\left(\frac{T}{J}\right)^{\alpha+1/2}, \tag{22}$$

where $\Gamma(z)$ and $\zeta(z)$ are the gamma function and the Rieman zeta function, respectively. Thus, for $T\ll\omega_c$ the one-phonon-assisted dephasing rate shows a power-law temperature dependence. Note that for our model of acoustic phonons ($\alpha=3$), $\Gamma_1^{(1)}$ increases quite steeply, namely, as $T^{7/2}$. From numerical evaluation of $\Gamma_1^{(1)}$ for a homogeneous chain with all dipole-dipole interactions, we have found that the exponent 7/2 is increased to 3.85, mainly as a consequence of logarithmic corrections in the exciton dispersion near the lower band edge.[33,34] If we go beyond the parabolic range of the energy spectrum, the growth becomes even steeper; the exponent then tends to 4, because the density of states becomes a constant towards the center of the band.

In the opposite limit $T\gg\omega_c$, the exponential in the denominator of Eq. (21) can be expanded in a Taylor series. Up to second order, one obtains

$$\Gamma_1^{(1)} = \frac{W_0^{(1)}}{2\pi(2\alpha-1)}\left(\frac{\omega_c}{J}\right)^{\alpha-1/2}\frac{T}{J}, \tag{23}$$

which simply reflects the linear high-temperature dependence of the mean occupation number $\bar{n}(\omega)$. Obviously, this scaling also holds in the presence of disorder.

B. Pure dephasing

We now turn to the temperature dependence of the pure dephasing rate $\Gamma_{\nu}^{(2)}=(1/2)W_{\nu\nu}^{(2)}$. As for a homogeneous aggregate this rate does not depend on the state index ν, we will simply denote it as $\Gamma_{\text{pure}}^{(2)}$. Using the explicit form of $\mathcal{F}^{(2)}(\omega,\omega')$ given by Eq. (17), we arrive at

$$\Gamma_{\text{pure}}^{(2)} = \frac{3}{2}\frac{W_0^{(2)}}{N+1}\left(\frac{T}{J}\right)^{2\alpha+1} \int_0^{\omega_c/T} dx \frac{x^{2\alpha}e^x}{(e^x-1)^2}. \tag{24}$$

From Eq. (24) it follows that for $T\ll\omega_c$ ($\omega_c/T\rightarrow\infty$),

$$\Gamma_{\text{pure}}^{(2)} = \frac{3}{2}\frac{W_0^{(2)}}{N+1}\Gamma(2\alpha+1)\zeta(2\alpha)\left(\frac{T}{J}\right)^{2\alpha+1}, \tag{25a}$$

while for $T\gg\omega_c$ ($\omega_c/T\rightarrow 0$),

$$\Gamma^{(2)}_{\text{pure}} = \frac{3}{2}\frac{W^{(2)}_0}{(2\alpha-1)(N+1)}\left(\frac{\omega_c}{J}\right)^{2\alpha-1}\left(\frac{T}{J}\right)^2. \tag{25b}$$

For the case of scattering on acoustic phonons ($\alpha=3$) and $T \ll \omega_c$, we thus arrive at $\Gamma^{(2)}_{\text{pure}} \propto T^7$. This temperature dependence resembles that for the pure dephasing of an isolated state of a point center, derived by McCumber and Sturge.[35] The only difference is that the exciton dephasing rate undergoes suppression by a factor of $N+1$ due to the motional narrowing effect. We note that this narrowing is not observed for one-phonon-assisted dephasing [see Eqs. (22) and (23)]. The T^2 scaling of $\Gamma^{(2)}_{\text{pure}}$ in the high-temperature limit ($T \gg \omega_c$) results from the square of the mean phonon occupation number involved in Eq. (17).

To conclude this section, we stress that the $T^{2\alpha+1}$ and T^2 scaling relations of the pure dephasing rate with temperature obtained here, also hold for disordered aggregates, because this result is determined only by the two-vibration spectral density $\mathcal{F}^{(2)}(\omega,\omega')$. The suppression factor, however, will then be determined by the exciton localization size, rather than the chain length.

C. Inelastic two-phonon-assisted dephasing

Finally, we analyze the dephasing rate of the superradiant state ($\nu=1$) resulting from the two-phonon inelastic scattering of excitons. This rate, which will be denoted as $\Gamma^{(2)}_{\text{inel}}$, is determined by the sum of scattering rates to all higher states, $\Gamma^{(2)}_{\text{inel}}=(1/2)\Sigma_{\mu\neq 1}W^{(2)}_{\mu 1}$. Using Eqs. (15) and (16), and making the same assumptions as in the case of one-phonon-assisted dephasing (Sec. IV A), we obtain

$$\Gamma^{(2)}_{\text{inel}} = \frac{W^{(2)}_0}{4\pi}\left(\frac{T}{J}\right)^{2\alpha+3/2}\int_0^{\omega_c/T}dx\int_0^{\omega_c/T}dy \times \frac{x^\alpha y^\alpha}{(e^x-1)(e^y-1)}\left[\frac{2e^y}{\sqrt{x-y}}\Theta(x-y)+\frac{1}{\sqrt{x+y}}\right]. \tag{26}$$

In the low-temperature limit, $T \ll \omega_c$ ($\omega_c/T \to \infty$), Eq. (26) yields

$$\Gamma^{(2)}_{\text{inel}} = \frac{\kappa W^{(2)}_0}{4\pi}\left(\frac{T}{J}\right)^{2\alpha+3/2}, \tag{27}$$

where the numerical factor κ is given by the double integral in Eq. (26), with both upper limits replaced by infinity. Comparing Eq. (27) with Eq. (25a), we see that $\Gamma^{(2)}_{\text{inel}}$ is characterized by a steeper temperature dependence than $\Gamma^{(2)}_{\text{pure}}$. In particular, for $\alpha=3$ the rate $\Gamma^{(2)}_{\text{inel}} \propto T^{15/2}$. This means that at higher temperatures the inelastic two-phonon channel of dephasing can compete with the elastic one (Sec. V B). In the high-temperature limit, $T \gg \omega_c$ ($\omega_c/T \to 0$), the rate $\Gamma^{(2)}_{\text{inel}}$ is proportional to T^2, which is the same scaling relation as in the case of pure dephasing [Eq. (25b)].

V. DISORDERED AGGREGATES

In this section, we will analyze the temperature dependence of the various dephasing contributions in the presence of disorder and their effect on the width of the J-band. As we will see (and already anticipated in Sec. III A), the dephasing rates are spread over a wide region, in particular, at low temperature. As a consequence, it is not clear *a priori* what value (mean, typical, or other) of these rates should be related to the homogeneous width of the absorption spectrum. Therefore, the width of the J-band was obtained by direct simulation of the absorption spectrum, using the calculated dephasing rates to broaden each of the exciton transitions in the band. Explicitly, we have

$$A(E) = \frac{1}{N}\left\langle \sum_\nu \frac{F_\nu}{\pi}\frac{\Gamma_\nu}{(E-E_\nu)^2+\Gamma_\nu^2}\right\rangle. \tag{28}$$

where $F_\nu=(\Sigma_{n=1}^N \varphi_{\nu n})^2$ is the dimensionless oscillator strength of the νth exciton state and $\Gamma_\nu=\gamma_\nu/2+\Gamma^{(1)}_\nu+\Gamma^{(2)}_\nu$ is the total homogeneous width of this state. Here, $\Gamma^{(1)}$ and $\Gamma^{(2)}$ are given by Eqs. (12) and (18), respectively, and $\gamma_\nu=\gamma_0 F_\nu$ is the radiative decay rate of state ν (γ_0 denotes the radiative constant of a monomer). In all the simulations, we will assume the limit $\omega_c \gg T$, which implies that $\omega_c \to \infty$ in Eqs. (11) and (16). As before, the angular brackets denote the average over the random realizations of the site energies $\{\varepsilon_n\}$. The resulting J-band width Δ was determined as the full width at half maximum (FWHM) of the thus calculated absorption spectrum. A similar approach has been used[36] to simulate the absorption spectrum of thiocarbocyanine dye 3,3′-disulfopropyl-5,5′-dichloro-9-ethylthiacarbocyanine (THIATS) aggregates[37] at room temperature.

A. One-phonon-assisted dephasing

In order to study fluctuations in the dephasing rates, we analyzed their statistics, focusing on the lowest exciton state for each randomly generated disorder realization. This choice was motivated by the fact that the low-lying states dominate the absorption spectrum. The dephasing rate of the lowest state is denoted $\Gamma^{(1)}_\uparrow$; its distribution, collected by considering 3×10^4 disorder realizations for chains of $N=500$ molecules and a disorder strength $\sigma=0.14J$ is presented in Figs. 1(a) and 1(b). In generating these figures, we used a one-vibration spectral density of the form Eq. (11), with $\alpha=3$. Furthermore, the rates were calculated for $T=0.06J$ [Fig. 1(a)] and $T=0.23J$ [Fig. 1(b)]; for the protoptypical aggregates of pseudoisocyanine ($J=600\ \text{cm}^{-1}$), this agrees with temperatures of 50 and 200 K, respectively. We note that the horizontal axis of the distributions is scaled by the average value $\bar{\Gamma}^{(1)}_\uparrow$, so that the value of $W^{(1)}_0$ does not affect the figures. Of course, this scaling renders the axis temperature dependent, because $\bar{\Gamma}^{(1)}_\uparrow$ strongly depends on T, as we will see below (Fig. 3).

These figures clearly demonstrate that the relative spread in $\Gamma^{(1)}_\uparrow$ may be considerable, in particular, at low temperatures. This may be understood from the local band-edge level structure of the disordered tight-binding Hamiltonian.[38] For temperatures smaller than the J-band width, the exciton scatters between discrete levels in the vicinity of the band edge that are localized in the same region of the chain. Both the energy spacing between these states and their localization size undergo large fluctuations: $\delta E_{\mu\nu} \sim E_{\mu\nu}$ and $\delta(\Sigma_{n=1}^N \varphi^2_{\mu n}\varphi^2_{\nu n}) \sim \Sigma_{n=1}^N \varphi^2_{\mu n}\varphi^2_{\nu n}$.[23] As a consequence, $\delta W^{(1)}_{\mu\nu}$

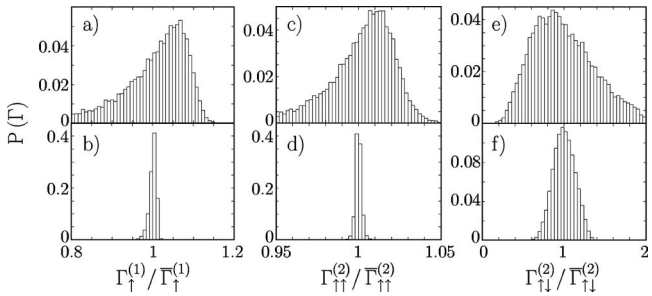

FIG. 1. Normalized distributions of the one-phonon-assisted and two-phonon-assisted dephasing rates $\Gamma^{(1)}_{\uparrow}$ [(a) and (b)], $\Gamma^{(2)}_{\uparrow\uparrow}$ [(c) and (d)], and $\Gamma^{(2)}_{\uparrow\downarrow}$ [(e) and (f)] of the lowest exciton state in each one of 3×10^4 disorder realizations for chains of 500 molecules. The upper panels correspond to $T=0.06J$, while the lower panels were calculated for $T=0.23J$. All plots were obtained for a disorder strength $\sigma=0.135J$ and a one- or two-vibration spectral density given by Eq. (11) or Eq. (16) with $\alpha=3$. Note that the horizontal axes are scaled by the average values of the three rates considered, indicated as $\bar{\Gamma}^{(1)}_{\uparrow}$, $\bar{\Gamma}^{(2)}_{\uparrow\uparrow}$, and $\bar{\Gamma}^{(2)}_{\uparrow\downarrow}$. These averages depend on temperature.

$\sim W^{(1)}_{\mu\nu}$. When the temperature is increased, the exciton in the lowest state may scatter to many higher-lying states, which often are delocalized over an appreciable part of the chain. This smears the fluctuations that occur in the scattering rates between individual states, leading to a decrease in the relative spread of the dephasing rate of the lowest state.

We next turn to the absorption band calculated according to Eq. (28), neglecting the role of two-phonon scattering $[W^{(2)}_0=0]$. In Fig. 2(a) this band is plotted for three temperatures at a fixed disorder strength of $\sigma=0.2J$. For the one-phonon spectral density we used the form of Eq. (22) with $W^{(1)}_0=25J$ and $\alpha=3$, and took $\gamma_0=1.5\times10^{-5}J$, which is typical for *J* aggregates of polymethine dyes. Chains of $N=500$ molecules were considered. The simulated spectra clearly demonstrate the thermal broadening, caused by growing homogeneous widths of the individual exciton transitions. At low temperature, the homogeneous broadening is negligible, the *J*-band is inhomogeneous, with a width that is determined by the disorder strength. With growing temperature, the *J*-band becomes more homogeneous, as is apparent from the fact that it gets more symmetric.

In Fig. 2(b) we plotted by symbols the simulated *J*-band width $\Delta(T)$ as a function of temperature for three values of the disorder strength: $\sigma=0.1J$, $0.2J$, and $0.3J$ [all other parameters were taken as in Fig. 2(a)]. As is seen, the $\Delta(T)$ shows a plateau at the value of the inhomogeneous width, $\Delta(0)=0.04J$, $0.1J$, and $0.18J$, respectively. Beyond these plateaus, $\Delta(T)$ goes up quite steeply, reflecting the fact that the homogeneous (dynamic) broadening becomes dominant. To accurately extract at low temperatures the small homogeneous contribution to the total width, we generated up to 4×10^5 disorder realizations. At higher temperatures, this number could be restricted to 4000, owing to the reduction of the relative fluctuations (cf. Fig. 1).

Inspired by the analytically obtained power laws for the one-phonon-assisted dephasing rate as a function of temperature for homogeneous aggregates (Sec. IV A), we considered a parametrization of the form

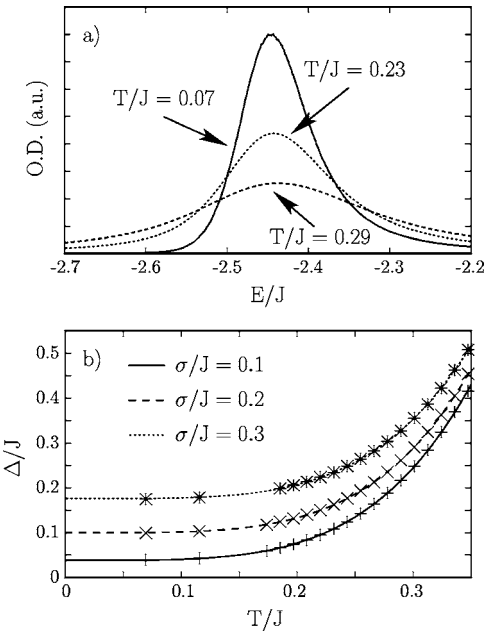

FIG. 2. (a) Calculated *J*-band for $T=0.07J$, $0.23J$, and $0.29J$ at a fixed disorder strength $\sigma=0.2J$. A one-phonon spectral density was used of the form Eq. (11), with $W^{(1)}_0=25J$ and $\alpha=3$, while the monomer radiative rate was set to $\gamma_0=1.5\times10^{-5}J$. (b) Temperature dependence of the width $\Delta(T)$ of the calculated *J*-band (symbols) for three values of the disorder strength, $\sigma=0.1J$, $0.2J$, and $0.3J$. Other parameters as in (a). The solid, dashed, and dotted curves represent the corresponding fits, according to Eq. (29).

$$\Delta(T)=\Delta(0)+aW^{(1)}_0(T/J)^p, \tag{29}$$

for the total bandwidth in disordered aggregates. It turned out that the calculated linewidths as a function of temperature could be fitted very well by the relation (29) [curves in Fig. 2(b)]. The corresponding fit parameters are $a=1.24$ and $p=4.16$ for $\sigma=0.1J$, $a=1.32$ and $p=4.29$ for $\sigma=0.2J$, and $a=1.20$ and $p=4.27$ for $\sigma=0.3J$. The scaling relation Eq. (29) turns out to hold over an even wider range of σ and W_0 values.[39] This implies that, although the *J*-band is built up from a distribution of exciton states with different dephasing rates, the total width $\Delta(T)$ may effectively be separated in an inhomogeneous width $\Delta(0)$ and a dynamic contribution.

We note that the fitting exponent *p* is larger than the value 3.85 found in the absence of disorder (Sec. IV A). This increase results from downward scattering processes between optically dominant exiton states, which are possible in the presence of disorder, but not for the superradiant state in the homogeneous chain. This claim may be substantiated by considering the dephasing rates of the lowest exciton state of each disorder realization. We numerically generated the average of this quantity, $\bar{\Gamma}^{(1)}_{\uparrow}$, from 3×10^4 disorder realizations for chains of $N=500$ molecules with $\sigma=0.1J$, $W^{(1)}_0=25J$, and $\alpha=3$. This average is shown as a function of temperature in Fig. 3 (diamonds), together with the dynamic contribution to the total *J*-band width, $\Delta(T)-\Delta(0)$ (solid line), and the dephasing rate $\Gamma^{(1)}_1$ of the superradiant state for a homogeneous chain of the same length (squares). As is seen, the dynamic part $\Delta(T)-\Delta(0)$ has a larger exponent $p=4.16$ than $\bar{\Gamma}^{(1)}_{\uparrow}$ ($p=3.85$). It is remarkable, however, that $\bar{\Gamma}^{(1)}_{\uparrow}$ and $\Gamma^{(1)}_1$ display almost identical behavior, at least in the relevant re-

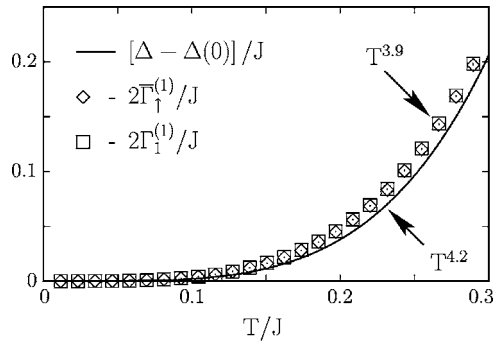

FIG. 3. Temperature dependence of two measures for the homogeneous width for disordered aggregates ($\sigma=0.1J$) compared to the dephasing rate of the lowest (superradiant) exciton state in a homogeneous aggregate ($\sigma=0$; squares). For the disordered case, we plotted the dynamic part $\Delta(T)-\Delta(0)$ of the total J-band width (solid line) and the average value $\bar{\Gamma}_{\uparrow}^{(1)}$ of the dephasing rate of the lowest exciton state found in each disorder realization (diamonds). In all cases we used a chain length of $N=500$, a monomer radiative rate of $\gamma_0=1.5\times10^{-5}J$, and a one-phonon spectral density of the form Eq. (11) with $W_0^{(1)}=25J$ and $\alpha=3$.

gion $T\gtrsim\Delta(0)$, where the homogeneous contribution to the J-band width is noticeable. For $T\ll\Delta(0)$, where $\Gamma_{\uparrow}^{(1)}$ undergoes significant fluctuations (see Fig. 1), $\bar{\Gamma}_{\uparrow}^{(1)}$ turns out to be much smaller than $\Gamma_1^{(1)}$. In the high-temperature regime, these fluctuations are washed out and the two quantities become almost identical.

So far, we have only presented the numerical results for one-phonon spectral density [Eq. (11)] with the power $\alpha=3$, which corresponds to a Debye model for the host vibrations. To end this subsection, we will address the effect of changing the spectral density. First, we consider the effect of the value for α. The diamonds in Fig. 4 present our results for the temperature dependence of the width $\Delta(T)$ obtained for $\alpha=1$ and $W_0=5J$. As before, we found that these data may be fitted by a simple power law of the form Eq. (29) (dashed line). In this case we find $p=1.9$, which, again, is slightly larger than the value of 3/2 found from Eq. (22), due to the correction of the dispersion relation arising from the long-range dipole-dipole interactions and downward scattering processes that contribute to the total J-band width. Clearly,

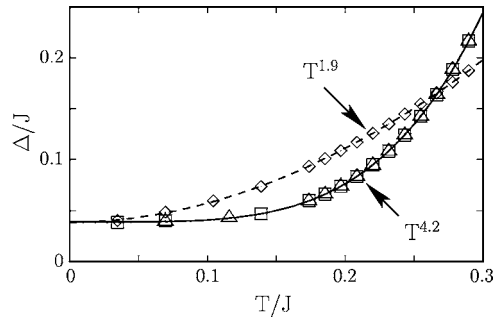

FIG. 4. Temperature dependence of the calculated width $\Delta(T)$ using three different models for the one-phonon spectral density. Diamonds (triangles) correspond to a spectral density of the form Eq. (11) with $\alpha=1$ and $W_0^{(1)}=5J$ ($\alpha=3$ and $W_0^{(1)}=25J$), while the squares are the results for $\mathcal{F}^{(1)}(\omega)=W_0^{(1)}(\omega/J)^3[1+\sin(2\pi\omega/\tilde{\omega})]$ with $W_0^{(1)}=25J$ and $\tilde{\omega}=J/6$. The various curves are fits to the power law [Eq. (29)]. In all cases we used a chain length of $N=500$ and a monomer radiative rate of $\gamma_0=1.5\times10^{-5}J$.

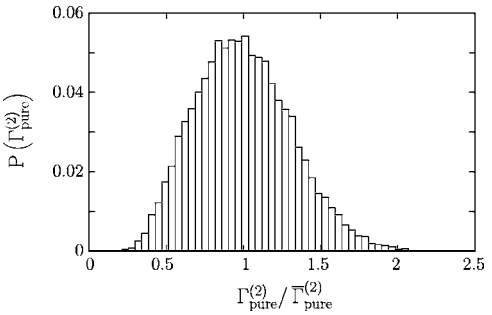

FIG. 5. As in Fig. 1, but now for $\Gamma_{\text{pure}}^{(2)}$. As discussed in the text, this distribution is solely due to the fluctuations in the inverse participation ratio of the exciton states and does not depend on temperature.

these data demonstrate the sensitivity of the temperature dependence of the total linewidth to the power α.

Interestingly, it turns out that while the temperature dependence of the J-band width is sensitive to the overall frequency scaling of the spectral density, it is not sensitive to fluctuations of this scaling around an average power law. To demonstrate this, we have considered a spectral density of the form $\mathcal{F}^{(1)}(\omega)=W_0^{(1)}(\omega/J)^3[1+\sin(2\pi\omega/\tilde{\omega})]$, which only on average exhibits an ω^3 dependence. The results for the width $\Delta(T)$ obtained for $W_0^{(1)}=25J$ and $\tilde{\omega}=J/6$ are presented as squares in Fig. 4. Remarkably, these results are indistinguishable from those obtained without fluctuations (i.e., $\tilde{\omega}=\infty$: triangles). The reason is that at elevated temperatures the function $\omega^3\bar{n}(\omega)$ varies slowly on the scale of $\tilde{\omega}$, so that the modulating function $1+\sin(2\pi\omega/\tilde{\omega})$ may be replaced by its average value, which equals unity.

B. Two-phonon-assisted dephasing

As we have seen in Sec. III B, the two-phonon-assisted dephasing rate $\Gamma_{\nu}^{(2)}$ consists of four contributions, one of which is elastic (indicated as "pure," as it is responsible for pure dephasing), while the other three are inelastic and are indicated as downward ($\downarrow\downarrow$), cross ($\uparrow\downarrow$), and upward ($\uparrow\uparrow$). In Figs. 1(c)–1(f), 5, and 6 we present the results for the statistics of these various contributions for disordered aggregates. In all cases, we used chains of 500 molecules, a disorder strength of $\sigma=0.135J$, and a two-vibration spectral density of the form Eq. (16), with $\alpha=3$. The statistics are presented for

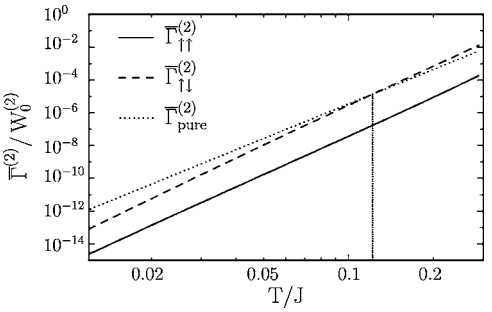

FIG. 6. Temperature dependence of the average values ($\bar{\Gamma}_{\uparrow\uparrow}^{(2)}$, $\bar{\Gamma}_{\uparrow\downarrow}^{(2)}$, and $\bar{\Gamma}_{\text{pure}}^{(2)}$) of the three contributions to the two-phonon-assisted dephasing rate of the lowest exciton state in disordered aggregates of $N=500$ molecules. Parameters were chosen as in Fig. 1. The vertical dotted line shows the crossing point at $T=0.12J$.

the lowest exciton state in each one of 3×10^4 randomly generated disorder realizations. For this state the downward contribution vanishes and the two-phonon-assisted dephasing rate reads $\Gamma_\nu^{(2)}=\Gamma_{\uparrow\uparrow}^{(2)}+\Gamma_{\uparrow\downarrow}^{(2)}+\Gamma_{\text{pure}}^{(2)}$. These three remaining contributions were calculated using the expressions derived in the Appendix.

From Figs. 1(c) and 1(d) we observe that at a given temperature, the relative spread in $\Gamma_{\uparrow\uparrow}^{(2)}$ is much smaller than that in $\Gamma_{\uparrow\downarrow}^{(2)}$. The reason is that in a two-phonon-assisted upward process the exciton in the lowest state scatters to more higher-energy states than in a cross process. As a result, fluctuations in $\Gamma_{\uparrow\uparrow}^{(2)}$ are suppressed more than those in $\Gamma_{\uparrow\downarrow}^{(2)}$. Upon heating, the spread of both $\Gamma_{\uparrow\uparrow}^{(2)}$ and $\Gamma_{\uparrow\downarrow}^{(2)}$ reduces, which has the same explanation as given for this effect in the case of one-phonon-assisted dephasing (Sec. V A). The distribution of $\Gamma_{\text{pure}}^{(2)}$ does not depend on temperature at all, because, according to Eq. (17), the rate $\Gamma_{\text{pure}}^{(2)}$ fluctuates exclusively due to fluctuations in the inverse participation ratio $\Sigma_{n=1}^{N}\varphi_{\nu n}^4$. As the latter quantity is subject to large fluctuations,[23] this also explains the large relative spread in $\Gamma_{\text{pure}}^{(2)}$.

In Fig. 6 we plotted (on a log-log scale) the temperature dependence of the mean values $\bar{\Gamma}_{\uparrow\uparrow}^{(2)}$, $\bar{\Gamma}_{\uparrow\downarrow}^{(2)}$, and $\bar{\Gamma}_{\text{pure}}^{(2)}$, obtained from averaging over these rates for the lowest exciton states in the simulations discussed above. This figure nicely shows the relative importance of the different dephasing channels. We clearly see that $\bar{\Gamma}_{\uparrow\uparrow}^{(2)}\ll\bar{\Gamma}_{\uparrow\downarrow}^{(2)},\bar{\Gamma}_{\text{pure}}^{(2)}$, i.e., the inelastic channel of dephasing due to double phonon absorption is inefficient, at all temperatures. More importantly, we observe that the cross channel of inelastic two-phonon-assited dephasing successfully competes with the pure dephasing contribution. At low temperatures, the pure dephasing dominates (it is, however, still negligible compared to the one-phonon-assisted dephasing), while at higher temperatures the inelastic cross process is more important. This correlates well with our findings for the disorder-free aggregates [see discussion below Eq. (27)]. For the disorder strength considered here, the crossover occurs at $T_0=0.12J$ ($\approx$100 K for $J=600$ cm^{-1}). We note that when considering two-phonon scattering, one often restricts to modeling the elastic process (see, e.g., Ref. 27). From the above we see that this is not justified at elevated temperatures.

Despite the fact that not all three curves in Fig. 6 are exactly straight lines (deviations occur in the unimportant low-temperature part), they all can be fitted very well by a power law, $a(T/J)^p$. In doing so, we obtained

$$\bar{\Gamma}_{\uparrow\uparrow}^{(2)}=0.18W_0^{(2)}(T/J)^{8.3}, \tag{30a}$$

$$\bar{\Gamma}_{\uparrow\downarrow}^{(2)}=9.01W_0^{(2)}(T/J)^{7.9}, \tag{30b}$$

$$\bar{\Gamma}_{\text{pure}}^{(2)}=1.88W_0^{(2)}(T/J)^{7}. \tag{30c}$$

We recall that the exponent $p=7$ in the last formula is an exact result for $\alpha=3$ and $\omega_c\gg T$, as was argued at the end of Sec. IV B already. As in the case of one-phonon scattering, we see that the inelastic two-phonon dephasing rates exhibit a steeper temperature dependence than for the homogeneous aggregate with nearest-neighbor interactions [Eq. (27)].

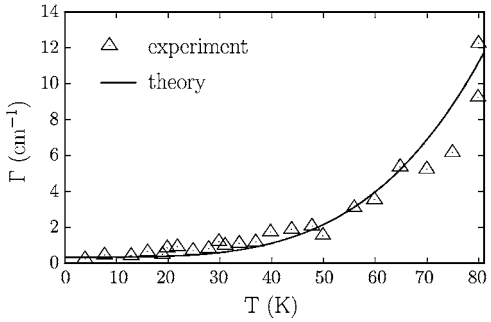

FIG. 7. Holewidth Γ as a function of temperature measured for aggregates of PIC-I after pumping in the center of the *J*-band (triangles). (Ref. 10). The solid line is our fit, assuming one-quantum scattering on acoustic phonons in the host. Model parameters are discussed in the text.

VI. COMPARISON TO EXPERIMENT AND DISCUSSION

It is of interest to see to what extent the model we presented here is able to explain the temperature dependence of the homogeneous broadening in molecular aggregates. As mentioned in the Introduction, Renge and Wild[11] found that the total *J*-band width $\Delta(T)$ of PIC-Cl and PIC-F over a wide temperature range (from 10 to 300 K) follows a power-law scaling as in Eq. (29). Although the power reported by these authors ($p=3.4$) is smaller than the ones we derived in Sec. V A, from direct comparison to the experimental data we have found that a model of one-phonon scattering with a spectral density given by Eq. (11) with $\alpha=3$ and $\omega_c\to\infty$ yields an excellent quantitative explanation of the experiments over the entire temperature range, both for the shape and the width of the *J*-band. The same turns out to be true for the *J*-band width of PIC-Br measured between 1.5 and 180 K.[7] In all these fits, σ and W_0 were the only two free parameters that could be adjusted to optimize the comparison to experiment. Details will be published elsewhere,[39] together with a fit of the much debated[7,40–43] temperature dependence of the fluorescence lifetime of these aggregates.

Here, we present an explicit comparison to the hole-burning data reported by Hirschmann and Friedrich.[10] Using this technique, they measured the homogeneous width of the exciton states in the center of the *J*-band for PIC-I over the temperature range of 350 mK–80 K. Their data for the holewidth Γ are reproduced as triangles in Fig. 7. The solid line shows our fit to these data, obtained by simulating disordered chains of $N=250$ molecules with a one-phonon spectral density of the form Eq. (11) with $\alpha=3$ and $\omega_c\to\infty$. The resonant interaction strength and the monomer radiative rate were chosen at the accepted values of $J=600$ cm^{-1} and $\gamma_0=1.5\times10^{-5}J=2.7\times10^8$ s^{-1}, respectively. Thus, the only free parameters were the disorder strength σ and scattering strength $W_0^{(1)}$. First, we fixed the value of σ by fitting the low-temperature (4 K) absorption spectrum, where the homogeneous broadening may be neglected. This yielded $\sigma=0.21J$. Next, $W_0^{(1)}$ was adjusted such that the measured growth of the hole width was reproduced in an optimal way. Thus, we found $W_0^{(1)}=180J$. For each given temperature the simulated holewidth was obtained as the FWHM of Eq. (28) where the summation over ν is restricted to those states that fall within the spectral interval covered by the laser used to burn the

hole. A study of the wavelength-dependent holewidths will be published elsewhere.[44] Here we restrict to burning at the *J*-band center and the comparison to experiment.

Taking into account the fair amount of scatter in the experimental data, we conclude from Fig. 7 that our model yields a good fit to the measurements. As mentioned above, the same holds for the *J*-band width in the aggregates of PIC-Cl, PIC-F, and PIC-Br. This yields valuable information about the dominant mechanism of dephasing in these materials. We conclude that this mechanism is one-phonon-assisted scattering of excitons on vibrations in the host characterized by a spectral density which (on average) scales as ω^3; this scaling yields a natural explanation of the power-law thermal broadening of the *J*-band found in various experiments. We stress that it is impossible to fit the experimental data with a spectral density that is constant or scales linearly with ω, as that yields considerably different power laws for the width [cf. Fig. 4]. The ω^3 scaling of the spectral density needed to fit the experiments strongly suggests that acoustic phonons dominate the scattering process. Thus, the spectral width measured over a broad temperature range is an excellent probe for the scattering mechanism.

It is appropriate to comment on the value of $W_0^{(1)}$ obtained from our fit, which seems to be very large. It should be kept in mind that $W_0^{(1)}$ is a phenomenological scattering strength, which combines several microscopic material properties [see discussion below Eq. (11)]. Most importantly, the value found here is consistent with a perturbative treatment of the scattering process: the scattering rates between the optically dominant states obtained from it turned out to be much smaller than their energy separation.

We finally address an alternative mechanism of dephasing, namely, scattering on local vibrations belonging to the aggregate. This has been suggested by several authors based on the activation-law fits of the measured homogeneous contribution to the *J*-band width.[7,10] To get an estimate whether this is a reasonable mechanism, let us neglect the disorder and make the nearest-neighbor approximation for the resonance interactions J_{nm}. Then, E_ν and $\varphi_{\nu n}$ are given by Eq. (19). Close to the lower exciton band edge, the region of our interest, $E_\nu = -2J + J\pi^2\nu^2/(N+1)^2$. Furthermore, let us parametrize the spectral function of a local vibration of frequency ω_0 as $\mathcal{F}(\omega) = 2\pi V_0^2 \delta(\omega - \omega_0)$, where V_0 is the coupling constant to the excitons. We are interested in the dephasing rate Γ_1 of the superradiant state $|\nu=1\rangle$. Using the above simpifications and replacing in Eq. (12) the summation over exciton states by an integration, one easily arrives at

$$\Gamma_1 = V_0^2 \frac{\bar{n}(\omega_0)}{(J\omega_0)^{1/2}}. \tag{31}$$

Comparing this result to the activation law $b\exp(-\omega_0/T)$, used in Refs. 7 and 10 to fit the experimental data, one obtains $V_0^2 = b(J\omega_0)^{1/2}$. Substituting the values $b = 3000\ \mathrm{cm}^{-1}$ and $\omega_0 = 330\ \mathrm{cm}^{-1}$ from Ref. 10, and $J = 600\ \mathrm{cm}^{-1}$, we obtain as estimate for the exciton-phonon coupling $V_0 \approx 1100\ \mathrm{cm}^{-1}$. This is an enormously large number. In particular, the Stokes losses $S = V_0^2/\omega_0 \approx 3700\ \mathrm{cm}^{-1}$ turn out to be much larger than the resonant interaction $J = 600\ \mathrm{cm}^{-1}$. Under these conditions, a strong exciton self-trapping is to be expected, resulting in a reduction of the exciton bandwidth by a factor of $\exp(-S/\omega_0) \ll 1$.[45] Coherent motion of the exciton, even over a few molecules, is then hardly possible: any disorder will destroy it. This observation is not consistent with the widely accepted excitonic nature of the aggregate excited states, as corroborated by many optical and transport measurements.[3,46]

VII. CONCLUDING REMARKS

In this paper we presented a theoretical study of the temperature dependence of the exciton dephasing rate in linear *J* aggregates and the resulting width of the total absorption band (the *J*-band). As dephasing mechanism we considered scattering of the excitons on vibrations of the host matrix, taking into account both one- and two-vibration scatterings. The excitons were obtained from the numerical diagonalization of a Frenkel exciton Hamiltonian with energy disorder and their dephasing rates were subsequently calculated using a perturbative treatment of the exciton-vibration interaction (Fermi golden rule).

In the absence of disorder, the lowest (superradiant) exciton state dominates the absorption spectrum. As a result, the dephasing rate of this state directly gives the homogeneous width of the *J*-band. We analytically calculated the temperature dependence of this homogeneous width for both one- and two-vibration scatterings, assuming a Debye-type model for the host vibration density of states. It turned out that in all cases the homogeneous width obeys a power law as a function of temperature, with the value of the exponent depending on the shape of the low-energy part of the vibronic spectrum (Sec. IV).

In the presence of disorder the optically dominant exciton states still reside close to the bottom of the band, but their energies are now spread and their wave functions become localized on finite segments of the chain. We have found that the various one- and two-phonon-induced contributions to the dephasing rate undergo significant fluctuations, because the exciton energies and overlap integrals vary considerably from one disorder realization to the other (Sec. V). As a consequence, one cannot use the dephasing rates of individual states to characterize the homogeneous broadening of the *J*-band. Instead, we simulated the total *J*-band and showed that its width effectively separates in an inhomogeneous (zero temperature) contribution and a dynamic (homogeneous) part. The latter scales with temperature according to a power law [Eq. (29)], with an exponent that is somewhat larger than the one found for the homogeneous broadening in the absence of disorder. We also showed that among the two-vibration scattering processes, inelastic channels will at elevated temperatures dominate the usually considered pure-dephasing contribution.

Finally, from comparison to absorption and hole-burning experiments (Sec. VI), we found that the dominant mechanism of dephasing for *J* aggregates lies in one-phonon scattering of excitons on vibrations of the host matrix, characterized by a spectral density which (on average) scales like the third power of the phonon frequency. This suggests that the

acoustic phonons of the host play an important role in the scattering process. All temperature-dependent data available to date are consistent with this picture. By contrast, we argued that the previously suggested mechanism of scattering on local vibrations of the aggregate, leading to an activated thermal behavior, is not consistent with the overwhelming amount of evidence that the optical excitations in *J* aggregates have an excitonic character.

ACKNOWLEDGMENT

This research is supported by the Materials Science Centre,[plus] a National Research Center financed by the Dutch Ministry of Education, Culture and Science, and by NanoNed, a national nanotechnology programme coordinated by the Dutch Ministry of Economic Affairs.

APPENDIX: TWO-PHONON SCATTERING RATES

In this Appendix we present the expressions for the two-phonon-assisted scattering rate $W_{\mu\nu}^{(2)}$, starting from Eq. (15). After substituting the two-vibration spectral density given in Eq. (16) and performing several algebraic manipulations, we arrive at

$$W_{\mu\nu}^{(2)} = W_0^{(2)}\left(\frac{T}{J}\right)^{2p+1}\sum_{n=1}^{N}\varphi_{\mu n}^2\varphi_{\nu m}^2[F_{\downarrow\downarrow}^{(2)}(\omega_{\mu\nu}) + 2F_{\uparrow\downarrow}^{(2)}(\omega_{\mu\nu}) + F_{\uparrow\uparrow}^{(2)}(\omega_{\mu\nu})], \tag{A1}$$

where the temperature-dependent functions $F_{\downarrow\downarrow}^{(2)}(\omega_{\mu\nu})$, $F_{\uparrow\downarrow}^{(2)}(\omega_{\mu\nu})$, and $F_{\uparrow\uparrow}^{(2)}(\omega_{\mu\nu})$ distinguish between the scattering processes in which two phonons are emitted ($\downarrow\downarrow$), one is absorbed and one is emitted ($\uparrow\downarrow$), and two phonons are absorbed ($\uparrow\uparrow$). They are given by

$$F_{\downarrow\downarrow}^{(2)}(\omega_{\mu\nu}) = \int_0^{\omega_c/T}dx\int_0^{\omega_c/T}dy f_{\downarrow\downarrow}(x,y)\,\delta\left(\frac{\omega_{\mu\nu}}{T}+x+y\right), \tag{A2a}$$

$$F_{\uparrow\downarrow}^{(2)}(\omega_{\mu\nu}) = \int_0^{\omega_c/T}dx\int_0^{\omega_c/T}dy f_{\uparrow\downarrow}(x,y)\,\delta\left(\frac{\omega_{\mu\nu}}{T}-x+y\right), \tag{A2b}$$

$$F_{\uparrow\uparrow}^{(2)}(\omega_{\mu\nu}) = \int_0^{\omega_c/T}dx\int_0^{\omega_c/T}dy f_{\uparrow\uparrow}(x,y)\,\delta\left(\frac{\omega_{\mu\nu}}{T}-x-y\right), \tag{A2c}$$

where, after changing to dimensionless integration variables $x=\omega_q/T$ and $y=\omega_{q'}/T$, we introduced the auxiliary functions,

$$f_{\downarrow\downarrow}(x,y) = \frac{x^p e^x}{e^x-1}\frac{y^p e^y}{e^y-1}, \tag{A3a}$$

$$f_{\uparrow\downarrow}(x,y) = \frac{x^p}{e^x-1}\frac{y^p e^y}{e^y-1}, \tag{A3b}$$

$$f_{\uparrow\uparrow}(x,y) = \frac{x^p}{e^x-1}\frac{y^p}{e^y-1}. \tag{A3c}$$

We note that for $\mu=\nu$ ($\omega_{\mu\nu}=0$), the only nonvanishing term is $F_{\uparrow\downarrow}^{(2)}(0)$, which describes the elastic channel of scattering (pure dephasing).

We now further analyze the three contributions to the scattering rate. As $\mathcal{F}_{\downarrow\downarrow}^{(2)}(\omega_{\mu\nu})$ describes the emission of two vibrational quanta, we have $\omega_{\mu\nu}<0$. Thus, performing the y integration, we obtain

$$F_{\downarrow\downarrow}^{(2)}(\omega_{\mu\nu}) = \int_0^{-\omega_{\mu\nu}/T}dx f_{\downarrow\downarrow}\left(x,-\frac{\omega_{\mu\nu}}{T}-x\right), \tag{A4a}$$

if $-\omega_{\mu\nu}<\omega_c$, and

$$F_{\downarrow\downarrow}^{(2)}(\omega_{\mu\nu}) = \int_{-(\omega_{\mu\nu}+\omega_c)/T}^{\omega_c/T}dx f_{\downarrow\downarrow}\left(x,-\frac{\omega_{\mu\nu}}{T}-x\right), \tag{A4b}$$

if $\omega_c<-\omega_{\mu\nu}<2\omega_c$, while $F_{\downarrow\downarrow}^{(2)}(\omega_{\mu\nu})=0$ otherwise.

Next, the contribution which involves the emission and absorption of one vibrational quantum is given by

$$F_{\uparrow\downarrow}^{(2)}(\omega_{\mu\nu}) = \int_{\omega_{\mu\nu}/T}^{\omega_c/T}dx f_{\uparrow\downarrow}\left(x,-\frac{\omega_{\mu\nu}}{T}+x\right), \tag{A5a}$$

if $0\leqslant\omega_{\mu\nu}<\omega_c$. If $0<-\omega_{\mu\nu}<\omega_c$,

$$F_{\uparrow\downarrow}^{(2)}(\omega_{\mu\nu}) = \int_0^{(\omega_c+\omega_{\mu\nu})/T}dx f_{\uparrow\downarrow}\left(x,-\frac{\omega_{\mu\nu}}{T}+x\right), \tag{A5b}$$

and $F_{\uparrow\downarrow}^{(2)}(\omega_{\mu\nu})=0$ otherwise.

Finally, the contribution that results from the absorption of two vibrational quanta ($\omega_{\mu\nu}>0$) yields

$$F_{\uparrow\uparrow}^{(2)}(\omega_{\mu\nu}) = \int_0^{\omega_{\mu\nu}/T}dx f_{\uparrow\uparrow}\left(x,\frac{\omega_{\mu\nu}}{T}-x\right), \tag{A6a}$$

if $0<\omega_{\mu\nu}<\omega_c$, and

$$F_{\uparrow\uparrow}^{(2)}(\omega_{\mu\nu}) = \int_{(\omega_{\mu\nu}-\omega_c)/T}^{\omega_c/T}dx f_{\uparrow\uparrow}\left(x,\frac{\omega_{\mu\nu}}{T}-x\right), \tag{A6b}$$

if $\omega_c<\omega_{\mu\nu}<2\omega_c$, while $F_{\uparrow\uparrow}^{(2)}(\omega_{\mu\nu})=0$ otherwise.

[1] E. E. Jelley, Nature (London) **138**, 1009 (1936); **139**, 631 (1937).
[2] G. Scheibe, Angew. Chem. **49**, 563 (1936); **50**, 212 (1937).
[3] *J-aggregates*, edited by T. Kobayashi (World Scientific, Singapore, 1996).
[4] J. Franck and E. Teller, J. Chem. Phys. **6**, 861 (1938).
[5] E. W. Knapp, Chem. Phys. **85**, 73 (1984).
[6] S. de Boer, K. J. Vink, and D. A. Wiersma, Chem. Phys. Lett. **137**, 99 (1987).
[7] H. Fidder, J. Knoester, and D. A. Wiersma, Chem. Phys. Lett. **171**, 529 (1990).
[8] H. Fidder, J. Terpstra, and D. A. Wiersma, J. Chem. Phys. **94**, 6895 (1991).
[9] H. Fidder, Ph.D. thesis, University of Groningen, NE, 1993.
[10] R. Hirschmann and J. Friedrich, J. Chem. Phys. **91**, 7988 (1989).
[11] I. Renge and U. P. Wild, J. Phys. Chem. A **101**, 7977 (1997).
[12] M. Shimizu, S. Suto, T. Goto, A. Watanabe, and M. Matsuda, Phys. Rev. B **58**, 5032 (1998).
[13] M. Shimizu, S. Suto, and T. Goto, J. Chem. Phys. **114**, 2775 (2001).
[14] M. Bednarz, V. A. Malyshev, and J. Knoester, Phys. Rev. Lett. **91**, 217401 (2003); J. Chem. Phys. **120**, 3827 (2004).
[15] A. V. Malyshev, V. A. Malyshev, and F. Domínguez-Adame, Chem. Phys. Lett. **371**, 417 (2003); J. Phys. Chem. B **107**, 4418 (2003).

[16] S. E. Dempster, S. Jang, and R. J. Silbey, J. Chem. Phys. **114**, 10015 (2001).
[17] I. Barvik, P. Reineker, Ch. Warns, and Th. Neidlinger, Chem. Phys. **240**, 173 (1999); *ibid.* **255**, 403 (2000).
[18] Ch. Warns, P. Reineker, and I. Barvik, Chem. Phys. **290**, 1 (2003).
[19] J. P. Lemaistre, J. Lumin. **83–84**, 229 (1999); **107**, 332 (2004).
[20] V. M. Agranovich and A. M. Kamchatnov, Chem. Phys. **245**, 175 (1999).
[21] M. Wubs and J. Knoester, Chem. Phys. Lett. **284**, 63 (1998).
[22] V. A. Malyshev, Opt. Spektrosk. **84**, 235 (1998) [Opt. Spectrosc. **84**, 195 (1998)].
[23] A. V. Malyshev and V. A. Malyshev, Phys. Rev. B **63**, 195111 (2001); J. Lumin. **94–95**, 369 (2001).
[24] A. S. Davydov, *Theory of Molecular Excitons* (Plenum, New York, 1971).
[25] M. Bednarz, V. A. Malyshev, and J. Knoester, J. Chem. Phys. **117**, 6200 (2002).
[26] T. T. Basiev, V. A. Malyshev, and A. K. Przhevuskii, in *Spectroscopy of Solids Containing Rare-Earth Ions*, edited by A. A. Kaplyanskii and R. M. MacFarlane (North-Holland, Amsterdam, 1987), p. 275.
[27] O. Kühn and V. Sundström, J. Chem. Phys. **107**, 4154 (1997).
[28] V. May and O. Kühn, *Charge and Energy Transfer Dynamics in Molecular Systems* (Wiley-VCH, Berlin, 2000).
[29] T. Renger, V. May, and O. Kühn, Phys. Rep. **343**, 137 (2001).
[30] B. Brüggemann, K. Szenee, V. Novoderzhkin, R. van Grondelle, and V. May, J. Phys. Chem. B **108**, 13536 (2004).
[31] K. Blum, *The Density Matrix Theory and Applications*, 2nd ed. (Plenum, New York, 1996).
[32] D. J. Thouless, Phys. Rep. **13**, 93 (1974).
[33] V. A. Malyshev and P. Moreno, Phys. Rev. B **51**, 14587 (1995).
[34] C. Didraga and J. Knoester, J. Chem. Phys. **121**, 946 (2004).
[35] D. E. McCumber and M. D. Sturge, J. Appl. Phys. **34**, 1682 (1963).
[36] D. M. Basko, A. N. Lobanov, A. V. Pimenov, and A. G. Vitukhnovsky, Chem. Phys. Lett. **369**, 192 (2003).
[37] I. G. Scheblykin, M. A. Drobizhev, O. P. Varnavsky, M. Van der Auweraer, and A. G. Vitukhnovsky, Chem. Phys. Lett. **261**, 181 (1996).
[38] V. A. Malyshev, Opt. Spektrosk. **71**, 873 (1991) [Opt. Spectrosc. **71**, 505 (1991)]; J. Lumin. **55**, 225 (1993).
[39] D. J. Heijs, V. A. Malyshev, and J. Knoester, Phys. Rev. Lett. (in press).
[40] S. de Boer and D. A. Wiersma, Chem. Phys. **131**, 135 (1989); Chem. Phys. Lett. **165**, 45 (1990).
[41] F. C. Spano, J. R. Kuklinsky, and S. Mukamel, Phys. Rev. Lett. **65**, 211 (1990); J. Chem. Phys. **94**, 7534 (1991).
[42] H. Fidder and D. A. Wiersma, Phys. Status Solidi B **188**, 285 (1995).
[43] E. O. Potma and D. A. Wiersma, J. Chem. Phys. **108**, 4894 (1998).
[44] D. J. Heijs, V. A. Malyshev, and J. Knoester, J. Lumin. (in press).
[45] E. I. Rashba, in *Excitons*, edited by E. I. Rashba and M. D. Sturge (North Holland, Amsterdam, 1982), p. 543.
[46] J. Knoester, in *Proceedings of the International School of Physics "Enrico Fermi,"* Course CXLIX, edited by V. M. Agranovich and G. C. La Rocca (IOS, Amsterdam, 2002), p. 149.